Materials Research. 2020; 23(2): e20190513
DOI: https://doi.org/10.1590/1980-5373-MR-2019-0513

A New Sensor Based on Reduced Graphene Oxide/Au Nanoparticles for Glycerol Detection

***Kelly Leite dos Santos Castro Assis*[a,b]*, *Braulio S. Archanjo*[a], *Carlos Alberto Achete*[a], *Eliane D'Elia*[b]**

[a]*Instituto Nacional de Metrologia, Qualidade e Tecnologia, Divisão de Metrologia de materiais, Duque de Caxias, RJ, Brasil.*
[b]*Universidade Federal do Rio de Janeiro, Instituto de Química, 21941-909, Rio de Janeiro, RJ, Brasil.*

Received: September 11, 2019; Revised: March 2, 2020; Accepted: April 7, 2020.

The projections for the global energy demand have been one of our society's greatest challenges, which has contributed significantly to the search for new sources of energy, among which biodiesel stands out and, consequently, the development of methods for quality assurance is essential to ensure its technological demand. In this context, a stable sensor based on graphene oxide and gold nanoparticles was developed for glycerol analysis. The electrochemically deposited gold nanoparticles presented the best results with a peak current (I_p) four times greater than the chemically produced gold nanoparticles. The combination of glassy carbon electrode with electrochemically reduced graphene and electrochemically deposited gold nanoparticles (GCE-ErGO-EAuNp) resulted in an efficient sensor to detect glycerol, promoting an I_p increase. The proposed non-enzymatic method showed a linear response in the concentration range of 1.0 x 10^{-3} to 1.0 x $10^{-2\%}$(w/w) with a good determination coefficient (r^2 = 0.9989), limits of detection and quantification at 1.2 x $10^{-4\%}$ and 4.0 x $10^{-4\%}$(w/w), respectively, with a repeatability of (RSD% ranged from 0.36% to 2.78%), intermediate precision and recovery of (99.3% to 104.4%) and excellent stability of 700 continuous analysis cycles.

Keywords: *Biodiesel, Liquid-liquid Extraction, Graphene Oxide, Gold Nanoparticles, Glycerol, Cyclic Voltammetry, Validation.*

1. Introduction

Glycerol is a water-soluble product that is viscous, hygroscopic, odourless and has a sweet taste; it is a natural chemical constituent of many foods and is currently used in fruit juices, wine, vegetable oil, beer, tobacco, honey, among others[1-4].

The determination of glycerol has been used in many applications, such as clinical, pharmaceutical and food-industry laboratories, and more recently in biodiesel quality control. There are several analytical methods in the literature for glycerol determination. The official methods for determining glycerol are those recommended by the Association of Official Analytical Chemists (AOAC) involving gas and liquid chromatography, which are time-consuming, tedious and expensive to use for routine analysis[3].

The development of accessible devices is necessary for the field's research advancement, which enables the development of alternative commercial techniques for the determination of this analyte. In this context, the enzymatic methods that combine the selectivity of enzymes involved are either 'in solution' or 'immobilized', and different detection systems have been extensively applied to develop prospective methods for measuring glycerol in clinical analysis, food products and biotechnological processes[4-13]. There is an enzymatic assay based on the methodology of substrate dosage by the end-point method that uses glycerokinase (GK) and glycerol-3-phosphate oxidase (G3PO) for glycerol analysis in different matrices such as tobacco casing, fermented products, blood serum and biodiesel[3,4,11,12,14].

Studies were recently presented in the literature about non-enzymatic electrochemical analysis through glycerol oxidation in NaOH solution at a boron-doped diamond electrode, gold electrode, copper electrode and Au(111)/SiO_2 cavity/ITO electrode[15-18]. As the electrochemical methods are cost effective, highly sensitive and mostly simple to perform, a search for new sensors is of the utmost importance[18]. A promising sensor material is graphene. This material presents high conductivity, surface area, thermal and mechanical stability[19-22]. Using reduced graphene oxide on electrochemical sensors promotes an increase of the sensor sensibility because of an increase of their current response[23-26].

Several catalysts can be found in the literature for the electro-oxidation of glycerol such as nickel, palladium, platinum, copper and gold[5,16,27-29].

The gold electrodes are considered very important for the free glycerol (FG) analysis in biodiesel, which has a wide linear range on the evaluation of glycerol concentration[18]. According to the Sabatier principle[30], a good catalyst must have an optimal adsorption force to yield a better activity. If the adsorption force is low, the adsorption step of the reagents is very slow, limiting the entire reaction. If the adsorption force is excessive, the catalyst does not release the products, which is a phenomenon

*e-mail: klcassis@gmail.com.

called catalyst poisoning and one of the main problems of the use of metals in organic molecules electroanalysis, generating the loss of electric signals as a result, which decreases the sensitivity of the electrode. In this context, the gold is an excellent catalyst for the electro-oxidation of organic molecules, like glycerol, because it promotes good stability and sensitivity. The reduced graphene oxide associated with gold is a promising combination for the development of a sensor for glycerol analysis, and this combination was studied in this work to analyze free glycerol contained in biodiesel.

In this study, sensors based on reduced graphene oxide (rGO) and gold nanoparticles (AuNp) were studied to detect free glycerol in biodiesel previously extracted by liquid phase extraction.

2. Experimental

2.1 Graphene Oxide Sample Preparation

For high yield and high performance of graphene oxide (GO) synthesized using a chemical route, the precursor requires a large surface area. Expanded graphite was used in this work as a precursor and was obtained from Nacional de Grafite. This precursor exhibits a larger surface area (21 BET/m^2 g^{-1}) than other precursors, such as graphite flakes (0.6 BET/ m^2 g^{-1}), due to the pre-treatment step[31,32]. Pre-treatment includes the intercalation of graphene sheets by small molecules followed by subsequent heating, which eliminates the intercalating molecules[32]. As a result, the recovered graphite exhibits considerably smaller crystallites, which lead to a significant increase in the surface area. Expanded graphite is a very bulky material that retains most of the properties of the original particles (graphite flakes), but gains additional processability or ability to be compressed into a highly cohesive, flexible sheet making it heat and chemically resistant. A precursor with a large surface area interacts easily with oxidant mixtures, which promotes higher yields. GO was prepared according to the Hummers' method[33].

Briefly, concentrated H_2SO_4 (9.2 mL) was added to a mixture of graphite (0.4 g) and $NaNO_3$ (0.2 g) in an ice bath. $KMnO_4$ (1.2 g) was slowly added to maintain the reaction temperature below 20 °C. The produced mixture was warmed up to 35 °C and stirred for 30 min. Subsequently, water (18.2 mL) was slowly added to the mixture; which promoted an intense exothermic reaction, increasing the temperature of the mixture to 98 °C. External heating was used to maintain the reaction temperature at 98 °C for 15 min. To stop the reaction, the mixture was initially placed in an ice bath for 10 min. Later, a solution containing water (55.3 mL) and 30% H_2O_2 (0.4 mL) were added. The product obtained was filtered and the resultant brown-coloured slurry was washed with HCl solution (180 mL of water and 20 mL of 30% HCl solution) to remove metallic ions residuals. The slurry placed in the HCl solution was then centrifuged to remove supernatant impurities. The remaining solution was repeatedly washed with water and centrifuged to remove impurities, until the pH of the supernatant water was neutral. Exfoliation of graphite oxide to GO was performed by the ultra-sonication of graphite oxide dispersions in water (1 mg mL^{-1})[34]. In our previous work, different processes of GO production were extensively studied to obtain a better proceeding for glassy carbon electrode (GCE) modification with rGO[34]. In this context, the GCE was modified with GO, exfoliated for 30 min on a probe sonicator(200 W) using the concentration of 1 mg mL^{-1}.

2.2 Characterization of expanded graphite and graphite oxide

Raman spectroscopy analyzes were carried out on a Renishaw InVia spectrometer with a 514.5 nm laser line at a power of 0.1 mW and 100x objective lens. All Raman spectra were obtained from accumulation and averaging of 10 scans with an accumulation time of 10 sec/scan and the reported spectra represent the average of twenty-five measurements made at different points of the sample.

X-ray diffraction (XRD) analysis was performed on a D8 Focus diffractometer (Bruker-AXS, Karlsruhe, Germany) with Ni-filtered Cu Kα characteristic radiation with a 2θ step of 0.02, and a collection time of 20s per step. A thin film of GO was prepared by dripping the sample suspension, 1:1 GO/water, onto a Si water and subsequently drying it in air.

Transmission-mode scanning electron microscopy (TSEM) images were acquired on a high-resolution SEM (Magellan 400).

FTIR analyses were performed using a Perkin–Elmer Spectrum GX spectrometer. The samples were prepared in powder form and mixed with potassium bromide (KBr) at a concentration of ~2 mg/g. The mixture was pressed into pellets of 1 mm thickness, applying 980 MPa equivalent pressures. The pellets were then analyzed in a spectrometer under ambient conditions in the range 400 cm^{-1} to 4000 cm^{-1} using 1 cm^{-1} of step and a resolution of 4 cm^{-1}. The final spectrum was an average of 16 scans.

2.3 Preparation of glassy carbon electrode modified with a reduced graphene oxide (GCE-rGO)

The GCEs used in this study were cleaned by polishing with alumina powder suspensions (1.0 and 0.3 μm), followed by rinsing with deionized water and sonication in 3mmol L^{-1} of HNO_3 for 5 min to remove alumina residues. GO-modified glassy carbon (GCE-GO) were prepared by dropping 10 μL of GO suspensions (1 mg mL^{-1}) onto the cleaned GCEs surface, followed by drying at 40 °C in an oven. Disc with a diameter of 3 mm of the GCE electrode limited the deposition volume of the GO solution.

Electrochemical reduction of GO cast on GCE-GO was carried out by chronoamperometry with a 0.1 mol L^{-1} phosphate buffer solution (PBS) solution at –1.2 V*versus* Ag/AgCl for 60 s, resulting in the formation of GCE-ErGO electrodes[35].

Thermal reduction of GO (TrGO) was carried out by the heat treatment in an oven at 300 °C for 1 hour followed by a treatment in a conventional microwave oven at 1000 W for 10 seconds. This methodology was established by Voiry et al.[36]. After reduction, the TrGO was dispersed in H_2O in a concentration of 1 mg $mL^{-1,}$ and 10 μL of this solution was deposited onto the cleaned GCEs surface, followed by drying at 40 °C in an oven.

2.4 Gold nanoparticles preparation

In the electrochemical method to prepare gold nanoparticles (EAuNp), the electrode was immersed in a solution containing 1mmol L^{-1} $HAuCl_4$ and 0.5 mol L^{-1} H_2SO_4. The electrodeposition occurred by applying potential cycles in the range of 0 to 850 mV with a scan rate of 12 V s^{-1} and 136 depositions[37]. After the Au deposition, the electrode was rinsed with Milli-Q water and oven dried at 40 °C. The electrochemical deposition of AuNp was performed on the GCE and GCE-ErGO modified.

In the colloidal method to AuNp production (QAuNp), 200 mL of MILI-Q H_2O at 100 °C, 7.5 mL of 1 mol L^{-1} sodium citrate and 7.5 mL of 1%w/w of $HAuCl_4$ were mixed and stirred for 8 minutes[38]. After the synthesis, the hot solution, which was still hot, was packed in a falcon tube to avoid fungi proliferation. The modification of GCE and GCE-ErGO was performed by dropped casting process using 10 µL of colloidal AuNp solution.

2.5 Characterization of GCE modified electrodes

The electrochemical performance of the produced electrodes using ErGO and TrGO (GCE-ErGO and GCE-TrGO) was studied by cyclic voltammetry (CV) in the potential range of -0.2 to 0.6 V, using potassium ferrocyanide (5 mmol L^{-1}), 0.1 mol L^{-1}KCl and 30 mV s^{-1} scan rate.

The electrochemical performance of the produced electrodes (GCE-ErGO-EAuNp and GCE-ErGO-QAuNp) towards glycerol (3 mmol L^{-1}) oxidation was studied by CV in the potential range of -0.5 to 0.6 V, with 30 mV s^{-1} scan rate in 0.2 mol L^{-1} KOH solution.

For the scan of electron microscopy (SEM) images and energy-dispersive X-ray spectroscopy (EDS) analyses, we have used a FEI Helios Nanolab 600 equipped with a Thermo Fisher EDS detector working at 10 kV and 50 pA for imaging and 3 nA for EDS.

2.6 Electrochemical cell

In all experiments, a platinum wire was used as the counter electrode, while an Ag/AgCl/KCl 3 mol L^{-1} was the reference electrode.

2.7 Partial validation of proposed method

The purpose of validating the studied method was to verify the reliability of the results; if it corroborates the requirements and standards for the specific proposed use. The parameters studied were: linearity, limit of detection (LOD), limit of quantification (LOQ), precision (repeatability and intermediate precision) and accuracy (recovery).

2.8 Linearity

The linearity study was performed by injection, in triplicate (n=3) of the standard solutions (k=10) corresponding to each point in the analytical curve. To test the homogeneity of variances, the Cochran test was used. The Cochran test verifies the differences between the variances of a given group of samples, and it was calculated according to Equation 1.

$$C = \frac{s_{max}^2}{\sum_{i=1}^{k} s_i^2} \quad (1)$$

Where: s_{max}^2 is the highest variance and $\sum_{i=1}^{k} s_i^2$ is the sum of all the variances of the samples.

The linearity was checked by the determination coefficient (r^2) of the curve. The working range was considered linear with values above 0.99[39].

2.9 Limit of detection and Limit of quantification

The limit of detection (LOD) was calculated following the evaluation of the standard deviation of the y-residuals from the line of best fit and slope of the analytical curve, through Equation 2 and the limit of quantification (LOQ) was obtained considering 3.3 times the value of LOD[39].

$$LOD = \frac{3\,s}{b} \quad (2)$$

Where: s is the standard deviation of the analytical curve intercept and b is the slope of the analytical curve.

The visual method was also performed to determine the LOD value.

2.10 Precision (repeatability and intermediate precision)

Precision was evaluated based on the repeatability of the analyses, which was analyzed from the standard deviations obtained in triplicate from an analytical curve constructed with the same instrument (Equation 3).

$$RSD\% = \frac{\sigma}{\bar{X}}.100 \quad (3)$$

Where: σ is the standard deviation of triplicate analyses and $\bar{X}$ is the results average.

The intermediate precision was evaluated through analysis of variances (ANOVA) with two analytical curves obtained with the same electrode and different electrodes plotted on different days, using the same experimental conditions (i.e., in the same laboratory and operating the same potentiostat). The Anova test evaluated the F value, whereas the slope comparison between the different curves was performed by the t test.

2.11 Accuracy (recovery)

Accuracy was reported as recovery, R (%), and it was verified for all concentrations, in triplicate, on the analytical curve. Results of accuracy were calculated according to Equation 4.

$$R(\%) = \frac{C_m}{C_{exp}}.100 \quad (4)$$

Where: C_m and C_{exp} are the measured and expected by the analytical curve concentrations, respectively.

2.12 Biodiesel analysis

For biodiesel analysis, a previous stage was performed to remove FG from the samples. This process was performed by liquid-liquid extraction using the method related in aprevious work of the group[3,4]. After the liquid-liquid extraction, the analysis by the proposed electrochemical method was carried out by adding a standard solution to the sample.

3. Results and Discussion

3.1 Sensors characterization and Glycerol electro-oxidation

The Figure 1 represents the structural and morphological characterization of the produced graphite oxide and the precursor, expanded graphite. The FTIR spectra is presented in Figure 1a, and shows evidences for the oxygen-containing functional groups in graphite oxide samples composed to physisorbed water or/and hydrogen bonds in 3500-3000 cm^{-1}, carbonyl groups in 1730 cm^{-1}, OH deformation in 1630 cm^{-1}, aromatic vibrations of C=C structure in 1580 cm^{-1} and vibrations of epoxy groups in 1183 cm^{-1}[25, 40]. The graphite structure presents a peak of physisorbed water and a peak of aromatic vibrations of C=C bonds.

The Raman spectra (Figure 1b) shows the broad G band at 1580 cm^{-1}, which is a result of in-plane vibrations of sp^2 bonded carbon atoms producing the E_{2g} symmetry normal mode[40,41]. The D band, in the graphite oxide structure, centered at 1350 cm^{-1} is A_{1g} symmetry mode produced by out-of-plane vibrations of carbon atoms, and it becomes active due to the presence of structural defects[41].

XRD measurements of the produced GO samples are shown in Figure 1c. The graphite oxide sample exhibits a characteristic XRD peak at $2\theta \approx 11°$ representing a periodic stacking of its sheets[42], unlike the graphite structure. It represents the modification of graphite structure after Hummers' process with a peak shift of 2θ of 26° to 11°.

Figure 1d shows TSEM micrograph, on dark field mode, of produced graphene oxide deposited on the ultrathin carbon film on a lacey carbon support film, which confirms the membrane-like architecture of GO, reproducing the results of similar studies on GO morphologies[33,34].

It is well known that electrical properties are fundamental to goodsensor performance. Along these lines, after the production of GOs two reduction procedures were carried out to produce reduced graphene oxide which, unlike graphene oxide, presents good electrical properties: with electrochemical and thermal reduction. Figure 2 shows all the electrochemical characterization of GCE modified with ErGO and TrGO in the presence of $K_3[Fe(CN)_6]$. It is noticed that both reduced materials have excellent performances regarding the GCE, showing higher responses of reduction and oxidation currents. However, the electrochemically reduced GO showed a current response, compared to the thermally reduced GO, two times higher, a fact that highlights its superior performance. The electrochemically reduced GO was obtained adding 10 μL of 1 mg L^{-1} graphene oxide dispersion in water on the GCE, and then it was reduced at -1.5 V/SCE. The TrGO was obtained in different way; the thermally reduced GO particles suspension in water were deposited on the GCE. This performance can be attributed to the little dispersion of the thermally reduced particles,

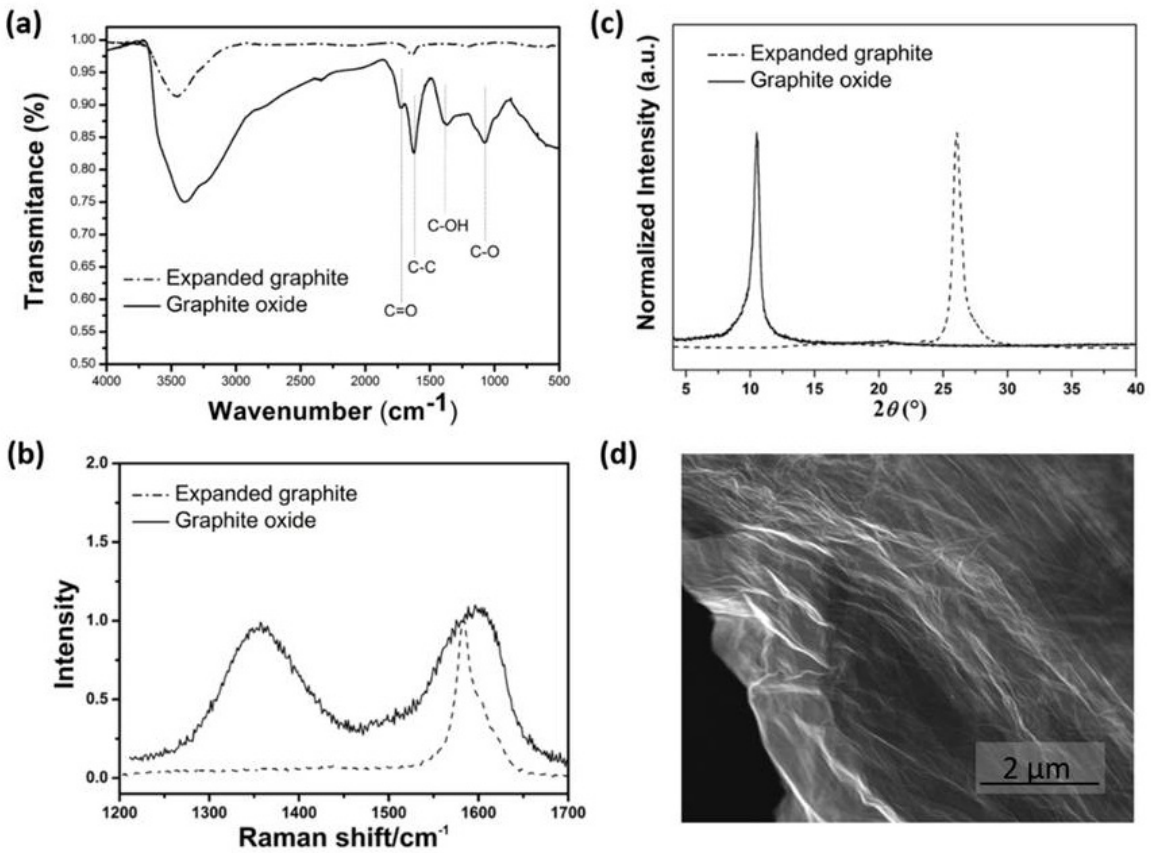

Figure 1. Graphite oxide structural and morphological characterization. FTIR (a), Raman (b), XRD (c) and STEM micrograph of produced graphite oxide (d).

because of the low solubility of the TrGO in an aqueous medium; and the graphene oxide presents a good dispersion in water. The solubility of TrGOs was higher in low polarity solvents such as hexane and toluene. On the other hand, the presence of these solvents on the electrode surface could reduce the electrode performance[43].

The best response of the ERGO electrode is probably because of the procedure used to prepare the electrode. In preparing the ERGO electrode an aliquot of GO dispersion is deposited on the glassy carbon electrode, while the TrGO electrode was obtained by adding an aliquot of TrGO suspension on the GCE. GO particles can disperse very well in water, whereas TrGO particles have little affinity for water. The GO particles deposited on the GCE were reduced at the surface, applying –1.5 V/SCE.

Figure 3 shows the electrochemical behavior of glycerol using GCE-ErGO in the presence and absence of glycerol. The small increase in the current is observed starting at 0.6 V in the presence of glycerol, which is, according to Tehrani et al. (2012) as related to the glycerol oxidation[29]. The insert in Figure 3 shows the behavior of GCE also in the absence and presence of glycerol. In comparison, the use of electrochemically reduced graphene (GCE-ErGO) promotes larger current responses. In the presence of glycerol, it was observed an increase of current in the GCE-ErGO electrode in more negative potential, showing its electro catalysis performance. The capacitive behavior of GCE-ErGO in relation to CGE relates to its large surface area. As previously described, the peak current (I_p) as well as the capacitive current (I_c) are proportional to the electrode area[34]. It can be shown that the metallic catalyst is fundamental to promote the electrochemical glycerol oxidation. Figure 3b shows the electro catalytic performance of AuNp towards glycerol oxidation. Two methods of AuNp production were tested: chemical synthesis and electrodeposition of a gold film directly on the electrode surface[37,44] (Figure 3b). As shown in Figure 3b, the electrochemical method of deposition showed the best results, providing a current about four times higher when compared to nanoparticles produced by the chemical method and dripped onto the surface. The ErGO-EAu-Np delivered more sensitivity than the ErGO-QAu-Np probably because of the presence of stabilizing ions (citrate) around theirparticles to avoid the crowding effect in the chemical synthesis. These large ions decrease the efficiency of the sensor towards the glycerol oxidation, because it makes the interaction between the Au nanoparticles and the glycerol molecules more difficult. The great advantages of using gold nanoparticles electrochemically deposited are: the possibility to achieve more homogeneous films, the films are prepared from dilute solutions that can be reused and a higher stability is achieved contrasting with the chemically obtained gold nanoparticles, which can generate larger aggregates when influenced by environmental and storage issues, such as temperature, pressure and external contamination.

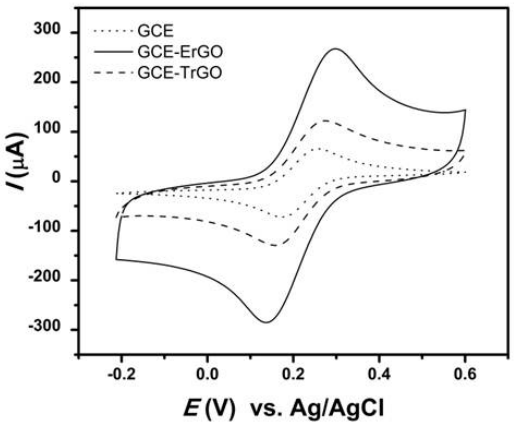

Figure 2. Cyclic voltammograms of GCE electrodes without modification, modified with TrGO (GCE-TrGO) and modified with ErGO (GCE-ErGO) in potassium ferrocyanide (5 mmol L^{-1}).

Figure 4a shows a comparison between GCE modified with EAuNp (GCE-EAuNp) and ErGO (GCE-ErGO-EAuNp). As noted, ErGO promoted an increase in I_p from 40 μA to 1000 μA, approximately. In fact, it can be attributed to the

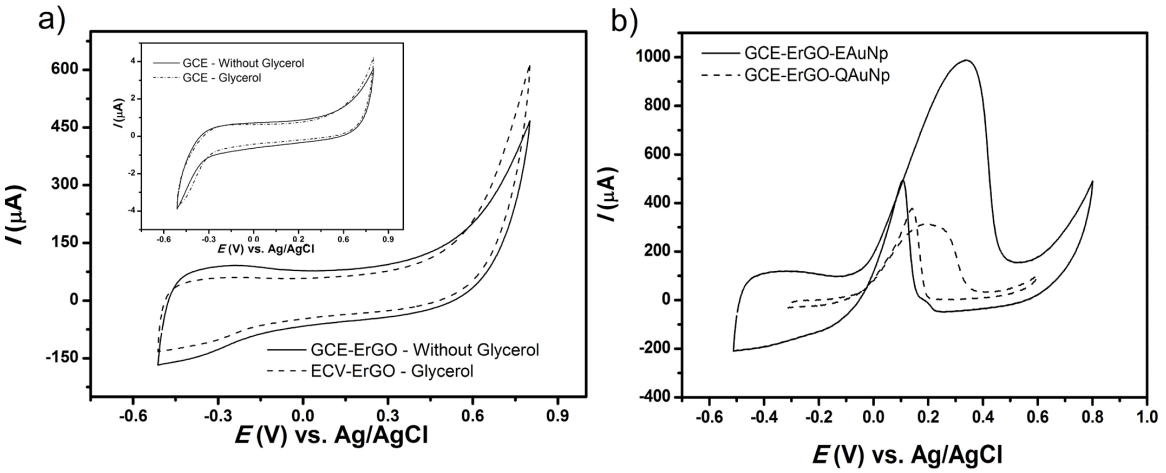

Figure 3. Cyclic voltammograms of GCE-ErGO without glycerol and with glycerol, the introduced graphic is the same analysis but using the CGE (a) and Cyclic voltammograms of GCE-ErGO modified with QAuNp and EAuNp (b), in 0.2 mol L^{-1} KOH solution containing 3 mmol L^{-1} glycerol using 30 mV s^{-1} scan rate.

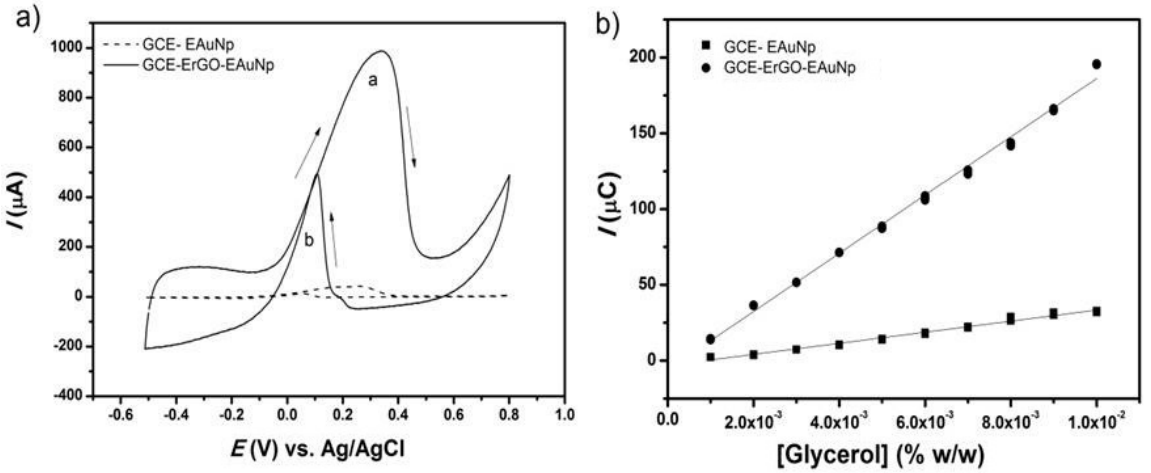

Figure 4. Cyclic voltammograms of GCE and EAuNp with (GCE-ErGO-EAuNp and without reduced graphene (GCE-EAuNp) modification in 0.2 mol L^{-1} KOH solution containing 3 mmol L^{-1} glycerol using 30 mV s^{-1} scan rate (a) and the respective analytical curves using GCE-EAuNp and GCE-ErGO-EAuNp (b).

increase of the active surface of the electrode promoted by ErGO. Figure 4b shows the influence of the use of ErGO on the I_p for different glycerol concentrations. The sensitivity improvement of the method is clear with the use of GCE-ErGO-EAuNp electrode.

The voltammetric profile of glycerol in gold electrodes is already well known in the literature[5,28]. The anodic peak, in Figure 4a, in the positive potential scan, is attributed to the electro-oxidation of the glycerol by the formation of its intermediates, in the reverse scan, another anodic peak is attributed to the oxidation of the remaining intermediates on the electrode surface. This peak in the reverse potential scan is responsible for electrode activation[28,45]. The mechanism for the electro-oxidation of glycerol in platinum was related for the first time in 1984[46] and confirmed in 1991 on gold electrodes[5]. It is described by a sequence of 4 reactions, presented below, being **M** the metallic working electrode, **G** the glycerol and the subscriber "**ads**" to the adsorbed substance (Equations 5-8). The formation of the AuOH species is necessary for the initiation of glycerol oxidation, since the electro-oxidation of glycerol on gold occurs through the interaction between adsorbed glycerol (Au-G_{ads}) and OH-adsorbed species ($AuOH_{ads}$). Among the products formed by the oxidation of glycerol are glyceraldehyde, tartronic acid and glyceric acid.

$$M + G \rightarrow M - G_{ads} \quad (5)$$

$$M - OH^{-} \rightarrow M - OH_{ads} + e- \quad (6)$$

$$M - G_{ads} + M - OH_{ads} \rightarrow products \quad (7)$$

$$M - G_{ads} + OH^{-} \rightarrow products + e- \quad (8)$$

Mohammad et al.[37] concluded that parameters such as scan rate and the number of cycles directly interfere with the size and homogeneity of the formed nanoparticles, which consequently decrease the electrode performance. The modified GCE with both ErGO and EAuNp presented homogeneous morphology, with excellent adhesion on the electrode surface and excellent stability.

Figure 5 shows SEM images of GCE: unmodified (Figure 5a), modified with ErGO (Figure 5b) and modified with both ErGO and EAuNp (Figure 5c and 5d), and the EDS chemical analyses (Figure 5e). Before modification, the GCE has a flat surface and some grooves (Figure 5a). After the ErGO modification, the presence of a wrinkled membrane on its surface, characteristic of the overlapping of ErGO sheets (Figure 5b), is observed. With the gold deposition, the characteristic of the ErGO film changes completely with the presence of several spherical shaped EAuNps (Figure 4c). A higher magnification SEM image (Figure 5d) shows the detail of the electro-deposited EAuNps having a bimodal distribution with mean sizes of about 20 nm and 100 nm. EDS analysis indicates a small amount of sodium on the surface of the CGE-ErGO (Figure 5e), which remains from thebuffer solution used in GO reduction. The film of the electrode showed the characteristic color of gold. Etesami and Mohamed[37] describe the same observation in Au electrochemically deposited on the surface of graphite.

4.2 Partial validation of the voltammetric method using GCE-ErGO-EAuNp as sensor for glycerol analysis

The partial validation is related by the evaluation of analytical Figures of merit such as sensitivity, linearity, limit of detection (LOD) and limit of quantification (LOQ), together with the accuracy and repeatability of the proposed method. The sensitivity was evaluated by the slope of the analytical curve (0.00673μC $(\%w/w)^{-1}$).

Figure 6a shows the cyclic voltammetric curves of GCE-ErGO-EAuNp for different glycerol concentrations (from $1.0x10^{-3}$ to $1.0x10^{-2}$% (w/w)) in 0.2 mol L^{-1} KOH. It can be observed that the increase in glycerol concentration led to a higher peak area. Thus, an analytical curve was constructed from the peak area data of the voltammetric

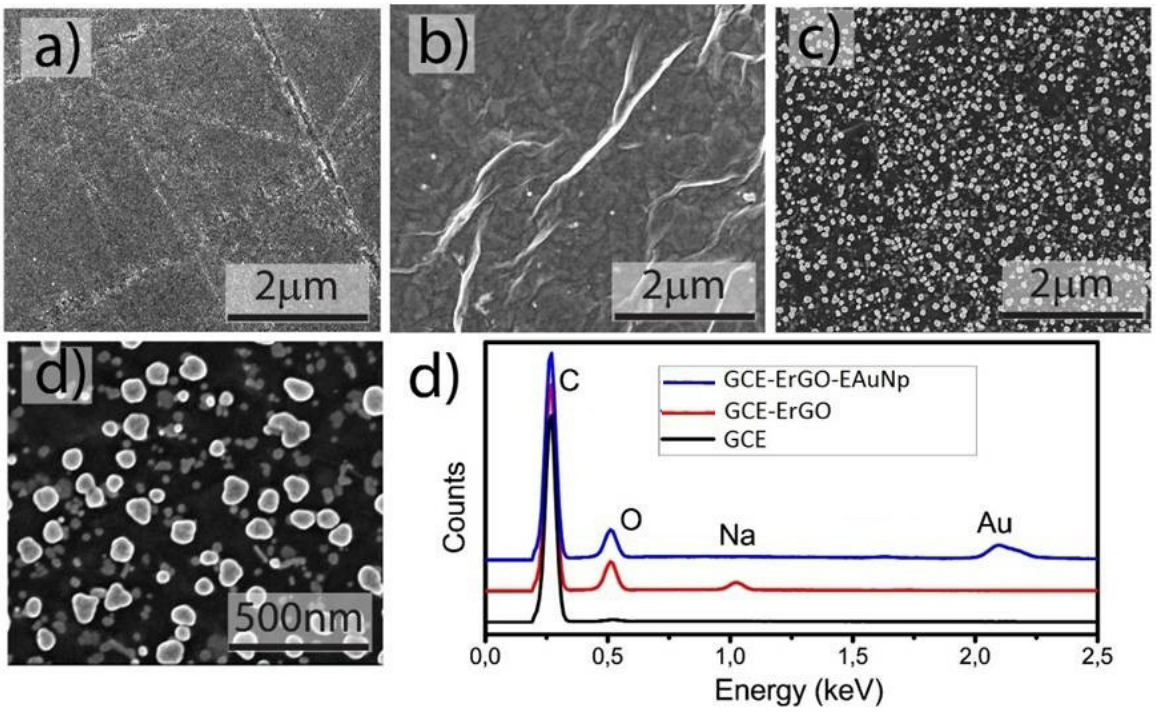

Figure 5. SEM images of the GCE: without modification (a), modified with ErGO (b) and finally with EAuNp (c). A higher magnification image of the GCE-ErGO-EAuNp (d) and EDS chemical analyses of the electrodes in all three steps (e).

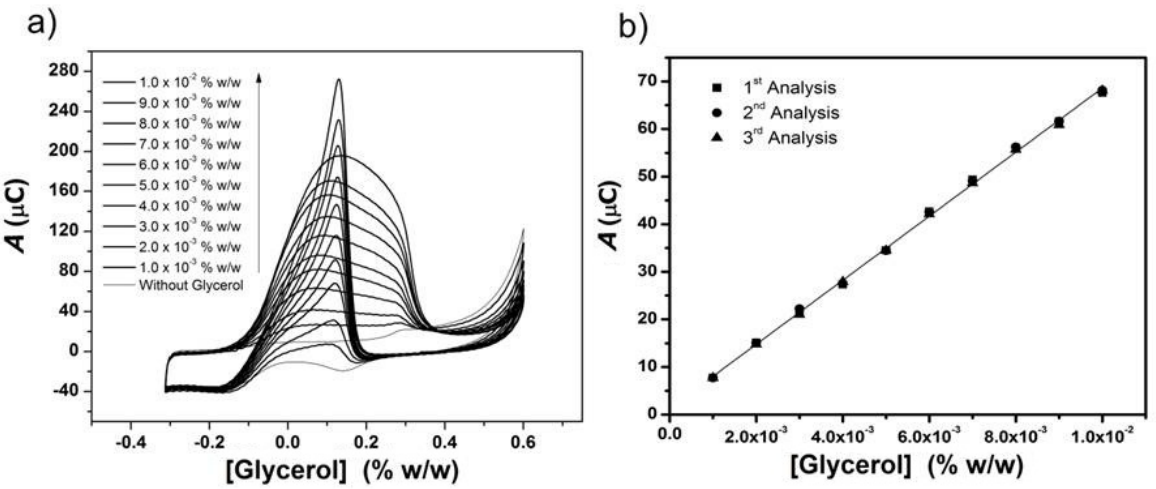

Figure 6. Cyclic voltammetric curves of GCE-ErGO-EAuNp for different glycerol concentrations to evaluate the linearity range of the method (a) and its analytical curve (b).

curves as a function of the glycerol concentration (Figure 6b). The choice of the peak area in the place of peak current is because of the enlargement of the peak, which is correlated to the various oxidation processes.

The peak area values obtained in triplicate for the linearity analysis were submitted to the Grubb's test (G) and no aberrant value was found.

This curve was submitted to the Cochran test to test for the bilateral deviation of the variances to a 5% significance level. This test evaluates the homogeneity of the variances. The calculated value (0.32) was also lower than the tabulated value (0.44) for the curve over the range of 1.0×10^{-3} to 1.0×10^{-2}% (w/w) (for k=10 and n=3), showing that the variances are homogeneous as the concentration increases, which characterizes an homoscedastic behavior. The analysis of the determination coefficient (r^2=0.9989) of the analytical curve indicated a linear relationship, with a linear correlation coefficient greater than 99%, and this value was considered adequate for this methodology[29,47].

Precision was evaluated based on the relative standard deviation of repeatability and from the intermediate precision. The relative standard deviation, shown in Table 1

for the analytical curve presented in Figure 4b, varied from 99.24 to 104.4%, which indicates that the method is acceptable and has a good repeatability.

The LOD and LOQ limits were also obtained by the statistical criteria. For this calculus the parameters found on the linearity study showed in Figure 5b was used. The LOD and LOQ found were $1.2x10^{-4}$ and $4.0x10^{-4}$% (w/w), respectively. These results corroborate with the visual LOD and LOQ values found as $1.0x10^{-4}$%(w/w) and $3.0x10^{-4}$% (w/w), respectively.

The intermediate precision of the method was evaluated from the analytical curves obtained using the same experimental conditions in different days (Figure 7a) and with different electrodes (Figure 7b).

The variances for the analytical curves obtained in different days, performed by the same analyst with the same ErGO-EAuNp (Figure 7a), presented a calculated F (0.005) lower than critic F (4.494), with a confidence of 95%. The comparison of the slopes of the straight lines shows the calculated (1.206) lower than critic t (2.306), with a confidence of 95%, revealing that the slopes of these two lines are equal.

The variances for the analytical curves obtained with different electrodes by the same analyst (Figure 7b), can be considered equal, since the calculated F value (0.39) is smaller than critic F(4.49). The slopes of the straight lines were also compared and found to be different straight lines, since the calculate t (6.33) is larger than the critic t (2.31), with a confidence of 95%. It means that it is necessary to build a new analytical curve for each new GCE-ErGO-EAuNp sensor.

In order to evaluate the stability of the electrode, several cycles of analysis were performed. A test with continuous cycles (700) was performed using GCE-ErGO-EAuNp sensor in 0.2 mol L^{-1} KOH containing 3 mmol L^{-1} of glycerol. The ECV-ErGO-EAuNp kept the peak current constant after 700 cycles of analysis.

A comparison between the sensor proposed in this work and other sensors reported in the literature that use gold or nickel as a catalyst for oxidation of glycerol is presented in Table 2. The method using Au electrode, flow injection analysis (FIA) and chronoamperometry (CA) detection showed an LOD in the range of 0.0005 mmol L^{-1}, the lowest LOD of the references cited in Table 2[15]. Despite the excellent LOD, the authors did not determine the free glycerol content in the biodiesel samples. They performed only a recovery study with biodiesel samples fortified with glycerol, and there was no comparative analysis with the reference method,

Table 1. Recovery results using the voltammetric method.

Theoretical [Glycerol] (% w/w)	1st Signal (μC)	2nd Signal (μC)	3rd Signal (μC)	Average (μC)	Standard deviation (μC)	Standard deviation (μC)	Measured [Glycerol] (% w/w)	Error (%)
1.0×10^{-3}	7.76×10^{-6}	7.71×10^{-6}	7.75×10^{-6}	7.74×10^{-6}	2.81×10^{-8}	0.36	1.01×10^{-3}	100.6
2.0×10^{-3}	1.51×10^{-5}	1.51×10^{-5}	1.48×10^{-5}	1.50×10^{-5}	2.10×10^{-7}	1.40	2.09×10^{-3}	104.4
3.0×10^{-3}	2.17×10^{-5}	2.22×10^{-5}	2.10×10^{-5}	2.17×10^{-5}	6.03×10^{-7}	2.78	3.08×10^{-3}	102.8
4.0×10^{-3}	2.73×10^{-5}	2.76×10^{-5}	2.79×10^{-5}	2.76×10^{-5}	3.05×10^{-7}	1.11	3.97×10^{-3}	99.3
5.0×10^{-3}	3.45×10^{-5}	3.44×10^{-5}	3.45×10^{-5}	3.45×10^{-5}	4.00×10^{-7}	0.12	5.00×10^{-3}	99.9
6.0×10^{-3}	4.27×10^{-5}	4.26×10^{-5}	4.21×10^{-5}	4.25×10^{-5}	3.01×10^{-7}	0.71	6.19×10^{-3}	103.2
7.0×10^{-3}	4.94×10^{-5}	4.91×10^{-5}	4.86×10^{-5}	4.91×10^{-5}	3.91×10^{-7}	0.80	7.17×10^{-3}	102.7
8.0×10^{-3}	5.60×10^{-5}	5.62×10^{-5}	5.57×10^{-5}	5.60×10^{-5}	2.69×10^{-7}	0.48	8.21×10^{-3}	102.6
9.0×10^{-03}	6.16×10^{-5}	6.17×10^{-5}	6.09×10^{-5}	6.14×10^{-5}	4.61×10^{-7}	0.75	9.01×10^{-3}	100.2
1.0×10^{-3}	6.76×10^{-5}	6.82×10^{-5}	6.81×10^{-5}	6.79×10^{-5}	3.24×10^{-7}	0.48	9.99×10^{-3}	99.9

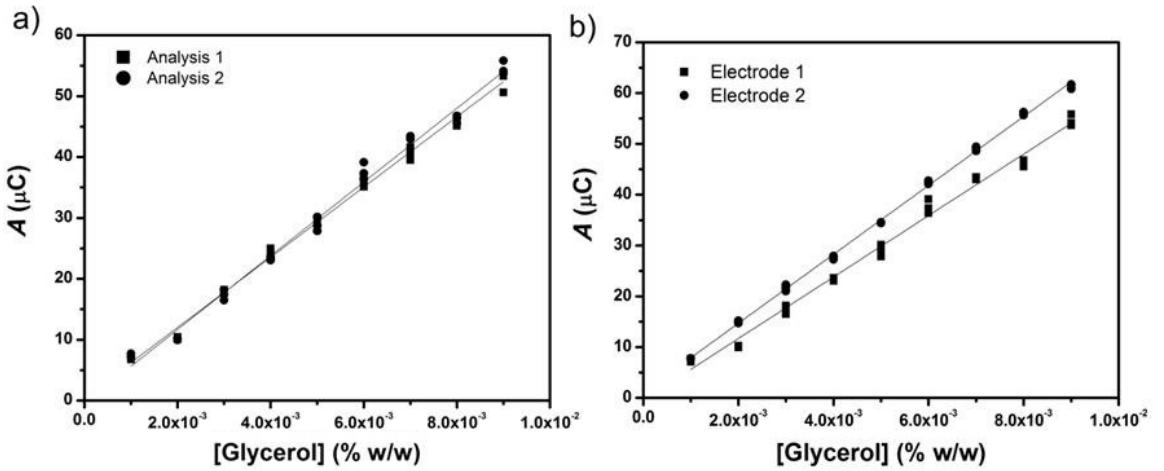

Figure 7. Analytical curves obtained by the same analyst using the same GCE-ErGO-EAuNp on different days (a) and analytical curves obtained by the same analyst using different GCE-ErGO-EAuNp (b).

Table 2. Comparison of analytical parameters for the proposed method with other electrochemical methods found in the literature.

Reference	Sensor	Electrochemical technique	LOD (mmol L^{1})	Linear range (mmol L^{-1})
Maruta and Paixão[16]	Au	FIA	0.0005	0.001 to 0.3
Li et al.[18]	Si/Au	VPD-CA	0.0015	0.01 to 0.8
Yasmin et al.[31]	C/NiNp	VPD-CA	0.033	0.5 to 12
Li et al.[18]	Cu	FIA-CA	0.003	0.033 to 1.7
Chen et al.[48]	PtRu-SPUME	CA	0.006	0.01 to 1
This Work	ErGO/EAuNp	CV	0.01	0.1 to 1.1

CV – cyclic voltammetry; DPA – differential pulse voltammetry; CA – chronoamperometry; FIA – flow injection analysis

gas chromatography. Others authors developed methods using FIA[18] or CA[48] methodologies and obtained lows LOD.

In contrast to the much smaller LOD achieved in this work, a LOD of 0.0015 mmol L^{-1} was reported in a method using silicon electrode with gold nanoparticles[18]. Actually, an ITO substrate, Indium Tin Oxide, was modified with polystyrene and SiO_2 from a colloidal silica dispersion. The aim of SiO_2 was to increase the surface area of the electrode for the gold nanoparticle deposition. Glycerol was analyzed using differential pulse voltammetry (DPV), the statistical study was not done and the stability of this electrode was not described.

Another method found in the literature used electrochemically deposited nickel nanoparticles on graphite-based electrode[29]. This work reached a LD of 0.033 mmol L^{-1} using DPV, three times higher than the LOD reached in this work.

Cyclic voltammetry was sensitive for the quantification of glycerol. Generally, this technique is used for qualitative analysis. For example, CA and DPV are the most used quantitative analyses. However, as previously discussed, the potential reverse scan is responsible for the reactivation of the electrode, since it oxidizes all remaining species from the main stage. It is already known in the literature that one of the great challenges of the electroanalysis of organic molecules is the deactivation of the electrode.

The electrodeposition of AuNp associated to the reduced graphene was able to provide a sensitive sensor for the analysis of the biodiesel quality, whose FG content should be a maximum of 0.02%(w/w), according to the regulatory agency. In addition, the excellent stability and resistance to poisoning of the sensor developed here makes it a great promise to glycerol analysis.

The matrix may contain components that interfere inthe sensor response, such alcohols used in biodiesel synthesis. These interferences may increase the electrochemicalsignal magnitude, and the level of the effect itself may depend on the concentration. The literature shows that gold in an alkaline medium presents an interesting characteristic regarding the other metals, and presents current densities variation according to the size of the alcohol molecule analyzed and the number of hydroxyl group[49,50]. The higher the number of a carbon chain, the higher is the current density[1,51], for example, methanol presents current densities lower than ethanol, which we attribute to an increasing hydrophobic character that would facilitate the displacement of water molecules from the interface[49,50]. Another point is the largest number of hydroxyl groups present in the molecule that promotes the increase in the current densities. This statement is confirmed in Figure 8.

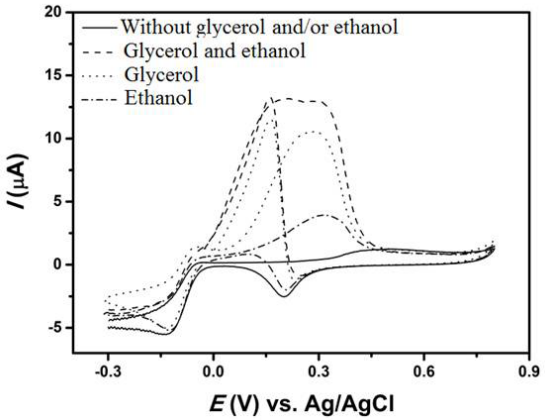

Figure 8. Selectivity test on GCE-ErGO-EAuNp sensor in the presence of ethanol (interfering).

The glycerol presents higher current density in relation to ethanol, besides the ethanol electro-oxidation occurs in a more positive potential comparing to glycerol. The Figure 8 shows that the mixture glycerol/ethanol presents the sum of the contributions of each alcohol, showing that the glycerol analysis should be performed by standard addition method and preferably removing the ethanol from the sample. Tehrani and Ghani (2012) also showed the influence of alcohols on the performance of glycerol analysis on modified electrodes with nickel nanoparticles[29] and attributed the recovery to be greater than 100% in the presence of alcohols, such as methanol or/and ethanol. To eliminate the interference in the glycerol recovery, a previously heating stage, on recovery studies, was performed to remove the methanol and ethanol residues leaving only the glycerol contribution.

4.3 Real sample analysis with the sensor proposed in this work

The method proposed herewas applied in the determination of FG in biodiesel samples, and the results are described in Table 3. Glycerol was extracted from biodiesel samples to aqueous phase according to literature[3]. After the liquid-liquid extraction, all samples were dried in a vacuum at 80°C to eliminate the residual alcohols and solvents. According to Figure 8 and the literature, sensors based on transition metals are not selective to alcohol molecules. The results obtained by standard addition method and the electrochemical method proposed here were compared to GC analysis. The data demonstrate that the extraction is effective because all the

Table 3. Comparison of free glycerol concentration in biodiesel samples obtained by CG and the electrochemical method proposed here.

Biodiesel Sample	GC (%w/w)	Electrochemical method (%w/w)	Recovery (%)
1	0.0060 ± 0.0005	0.0060 ± 0.0002	99.84
2	0.0180 ± 0.0005	0.0174 ± 0.0005	96.82
3	0.0019 ± 0.0005	0.0018 ± 0.0001	96.82

glycerol present in biodiesel was recovered. The data obtained by the electrochemical method proposed here also showed good recovery, ranging from 94.7 to 96.7%, demonstrating good recovery of free glycerol in biodiesel.

5.Conclusions

The glycerol analysis by the voltammetric method using glassy carbon electrode, modified with the electrochemically reduced graphene oxide with electrochemical deposition of gold nanoparticles, showsa linear response in glycerol concentration range of $1.0x10^{-3}$ to $1.0x10^{-1}$% (w/w). The detection and quantification limits obtained by the visual method were $1.0x10^{-4}$ and $3.3x10^{-4}$% (w/w), respectively and the detection and quantification limits obtained from the experimental data of the analytical curve were $1.2x10^{-4}$ and $4.0x10^{-4}$%(w/w), respectively. The low standard deviation of the analytical curve is responsible for the closeness value obtained by the visual and statistical methods.

The statistics showed a homogeneous bilateral variance deviation, and the method was considered homoscedastic. However, for the analytical curves obtained by different electrodes (identically prepared) the variance showed different slopes. These results demonstrated the necessity of a new analytical curve for each new electrode.

Finally, the development of an efficient and low-cost sensorsas an alternative to the chromatography method is very important. At this point, CGE-ErGO-EAuNp is presented as a promising alternative to the free glycerol detection in biodiesel, since the results obtained here certify that our method is exceptional with a good signal-to-noise ratio, linearity, short response time, good detection limit and excellent stability.

6. Acknowledgements

This work was supported by FAPERJ (Foundation for Research Support of the State of Rio de Janeiro) and Peugeot (E-26/111.159/2014).

7. References

1. Adzic RR, Hsiao MW, Yeager EB. Electrochemical oxidation of glucose on single crystal gold surfaces. J Electroanal Chem Interfacial Electrochem. 1989;260(2):475-85. http://dx.doi.org/10.1016/0022-0728(89)87164-5.
2. Souza FC, Vasconcellos FJ Jr, Cabral RC, Fernández TL, D'Elia E. Simple enzymatic methods for glycerol analysis in commercial beverages. Journal of Food. 2013;11(3):270-6. http://dx.doi.org/10.1080/19476337.2012.732613.
3. Luetkmeyer T, Santos RM, Silva AB, Amado RS, Castro Vieira E, D'Elia E. Analysis of free and total glycerol in biodiesel using an electrochemical assay based on a two-enzyme oxygen-electrode system. Electroanalysis. 2010;22(9):995-9. http://dx.doi.org/10.1002/elan.200900428.
4. Pêgas MM, Amado RS, de Castro EV, D'Elia E. Analysis of free glycerol in biodiesel using an electrochemical assay based on a two-enzyme platinum microelectrode system. J Appl Electrochem. 2010;40(11):2061-3. http://dx.doi.org/10.1007/s10800-010-0168-9.
5. Avramov-Ivić ML, Leger JM, Lamy C, Jović VD, Petrović SD. The electro-oxidation of glycerol on the gold(100)-oriented single-crystal surface and poly crystalline surface in 0.1 M NaOH. J Electroanal Chem Interfacial Electrochem. 1991;308(1-2):309-17. http://dx.doi.org/10.1016/0022-0728(91)85075-Z.
6. Merchie B, Girard A, Maisterrena B, Michalon P, Couturier R. Reliable amperometric determination of glycerol and glycerol-3-phosphate with a bienzymatic nylon membrane electrode. Anal Chim Acta. 1992;263(1-2):85-91. http://dx.doi.org/10.1016/0003-2670(92)85429-A.
7. Prodromidis MI, Stalikas CD, Tzouwara-Karayanni SM, Karayannis MI. Determination of glycerol in alcoholic beverages using packed bed reactors with immobilized glycerol dehydrogenase and an amperometric FIA system. Talanta. 1996;43(1):27-33. http://dx.doi.org/10.1016/0039-9140(95)01701-1. PMid:18966459.
8. Compagnone D, Esti M, Messia MC, Peluso E, Palleschi G. Development of a biosensor for monitoring of glycerol during alcoholic fermentation. Biosens Bioelectron. 1998;13(7-8):875-80. http://dx.doi.org/10.1016/S0956-5663(98)00055-4. PMid:9828385.
9. Niculescu M, Mieliauskiene R, Laurinavicius V, Csöregi E. Simultaneous detection of ethanol, glucose and glycerol in wines using pyrroloquinoline quinone-dependent dehydrogenases based biosensors. Food Chem. 2003;82(3):481-9. http://dx.doi.org/10.1016/S0308-8146(03)00118-3.
10. Katrlík J, Mastihuba V, Voštiar I, Šefčovičová J, Štefuca V, Gemeiner P. Amperometric biosensors based on two different enzyme systems and their use for glycerol determination in samples from biotechnological fermentation process. Anal Chim Acta. 2006;566(1):11-8. http://dx.doi.org/10.1016/j.aca.2006.02.063.
11. Gamella M, Campuzano S, Reviejo AJ, Pingarrón JM. Integrated multienzyme electrochemical biosensors for the determination of glycerol in wines. Anal Chim Acta. 2008;609(2):201-9. http://dx.doi.org/10.1016/j.aca.2007.12.036. PMid:18261515.
12. Minakshi, Pundir CS. Construction of an amperometric enzymic sensor for triglyceride determination. Sens Actuators B Chem. 2008;133(1):251-5. http://dx.doi.org/10.1016/j.snb.2008.02.036.
13. Goriushkina TB, Shkotova LV, Gayda GZ, Klepach HM, Gonchar MV, Soldatkin AP, et al. Amperometric biosensor based on glycerol oxidase for glycerol determination. Sens Actuators B Chem. 2010;144(2):361-7. http://dx.doi.org/10.1016/j.snb.2008.11.051.
14. Montoya A, March C, Mocholí A, Abad A, Manclús JJ, Ferrero JM. Electrochemical assays based on enzyme-electrode systems to determine glycerol and propylene glycol in tobacco casing. Sens Actuators B Chem. 1993;16(1-3):429-34. http://dx.doi.org/10.1016/0925-4005(93)85222-V.
15. Barbosa TGG, Richter EM, Muñoz RAA. Flow-injection pulsed-amperometric determination of free glycerol in biodiesel at a gold electrode. Electroanalysis. 2012;24(5):1160-3. http://dx.doi.org/10.1002/elan.201100719.
16. Maruta AH, Paixão TRLC. Flow injection analysis of free glycerol in biodiesel using a copper electrode as an amperometric

detector. Fuel. 2012;91(1):187-91. http://dx.doi.org/10.1016/j.fuel.2011.06.071.

17. Pop A, Manea F, Radovan C, Dascalu D, Vaszilcsin N, Schoonman J. Non-enzymatic electrochemical detection of glycerol on boron-doped diamond electrode. Analyst. 2012;137(3):641-7. http://dx.doi.org/10.1039/C2AN15645H. PMid:22159176.
18. Li N, Zhou Q, Li X, Chu W, Adkins J, Zheng J. Electrochemical detection of free glycerol in biodiesel using electrodes with single gold particles in highly ordered SiO_2 cavities. Sens Actuators B Chem. 2014;196(Suppl. C):314-20. http://dx.doi.org/10.1016/j.snb.2014.02.017.
19. Ali F, Agarwall N, Nayak PK. R. Das and N. Periasamy: chemical route to the formation of graphene. Curr Sci. 2009;97(5):683.
20. Dreyer DR, Park S, Bielawski CW, Ruoff RS. The chemistry of graphene oxide. Chem Soc Rev. 2010;39(1):228-40. http://dx.doi.org/10.1039/B917103G. PMid:20023850.
21. Park S, Ruoff R. Chemical methods for the production of graphenes. Nat Nanotechnol. 2009;4(4):217. http://dx.doi.org/10.1038/nnano.2009.58. PMid:19350030.
22. Chua CK, Pumera M. Chemical reduction of graphene oxide: a synthetic chemistry viewpoint. Chem Soc Rev. 2014;43(1):291-312. http://dx.doi.org/10.1039/C3CS60303B. PMid:24121318.
23. Kumar U, Yadav BC. Development of humidity sensor using modified curved MWCNT based thin film with DFT calculations. Sens Actuators B Chem. 2019;288:399-407. http://dx.doi.org/10.1016/j.snb.2019.03.016.
24. Kumar K, Kumar U, Singh M, Yadav BC. Synthesis and characterizations of exohedral functionalized graphene oxide with iron nanoparticles for humidity detection. J Mater Sci Mater Electron. 2019;30(14):13013-23. http://dx.doi.org/10.1007/s10854-019-01663-9.
25. Kumar U, Yadav BC. Synthesis of carbon nanotubes by direct liquid injection chemical vapor deposition method and its relevance for developing an ultra-sensitive room temperature based CO_2 sensor. Journal of the Taiwan Institute of Chemical Engineers. 2019;96:652-63. http://dx.doi.org/10.1016/j.jtice.2019.01.002.
26. Honório GG, Cunha JN, Assis KLSC, Aguiar PF, Andrade DF, Souza CG, et al. Free glycerol determination in biodiesel samples using palladium nanoparticles modified glassy carbon electrode associated with solid phase extraction. J Solid State Electrochem. 2019;23(11):3057-66. http://dx.doi.org/10.1007/s10008-019-04387-2.
27. Kwon Y, Lai SCS, Rodriguez P, Koper MTM. Electrocatalytic oxidation of alcohols on gold in alkaline media: base or gold catalysis? J Am Chem Soc. 2011;133(18):6914-7. http://dx.doi.org/10.1021/ja200976j. PMid:21504194.
28. Razmi H, Habibi E, Heidari H. Electrocatalytic oxidation of methanol and ethanol at carbon ceramic electrode modified with platinum nanoparticles. Electrochim Acta. 2008;53(28):8178-85. http://dx.doi.org/10.1016/j.electacta.2008.06.033.
29. Tehrani RMA, Ab Ghani S. Electrocatalysis of free glycerol at a nanonickel modified graphite electrode and its determination in biodiesel. Electrochim Acta. 2012;70(Suppl. C):153-7. http://dx.doi.org/10.1016/j.electacta.2012.03.044.
30. Deutschmann O, Knözinger H, Kochloefl K, Turek T. (2011). Heterogeneous catalysis and solid catalysts. In: Elvers B, editor. *Ullmann's encyclopedia of industrial chemistry* (1st ed.). Weinheim: Wiley.
31. Yasmin A, Luo J-J, Daniel IM. Processing of expanded graphite reinforced polymer nanocomposites. Compos Sci Technol. 2006;66(9):1182-9. http://dx.doi.org/10.1016/j.compscitech.2005.10.014.
32. Sun L, Fugetsu B. Mass production of graphene oxide from expanded graphite. Mater Lett. 2013;109:207-10. http://dx.doi.org/10.1016/j.matlet.2013.07.072.
33. Marcano DC, Kosynkin DV, Berlin JM, Sinitskii A, Sun Z, Slesarev A, et al. Improved synthesis of graphene oxide. ACS Nano. 2010;4(8):4806-14. http://dx.doi.org/10.1021/nn1006368. PMid:20731455.
34. Castro KLS, Oliveira SM, Curti RV, Araújo JR, Sassi LM, Almeida CM, et al. Electrochemical response of glassy carbon electrodes modified using graphene sheets of different sizes. Int J Electrochem Sci. 2018;13:71. http://dx.doi.org/10.20964/2018.01.02.
35. Camargo MNL, Santhiago M, Maroneze CM, Silva CCC, Timm RA, Kubota LT. Tuning the electrochemical reduction of graphene oxide: structural correlations towards the electrooxidation of nicotinamide adenine dinucleotide hydride. Electrochim Acta. 2016;197:194-9. http://dx.doi.org/10.1016/j.electacta.2015.09.022.
36. Voiry D, Yang J, Kupferberg J, Fullon R, Lee C, Jeong HY, et al. High-quality graphene via microwave reduction of solution-exfoliated graphene oxide. Science. 2016;353(6306):1413-6. http://dx.doi.org/10.1126/science.aah3398. PMid:27708034.
37. Etesami M, Mohamed N. Catalytic application of gold nanoparticles electrodeposited by fast scan cyclic voltammetry to glycerol electrooxidation in alkaline electrolyte. Int J Electrochem. 2011;6(10):4676-89.
38. Balasubramanian SK, Yang L, Yung L-YL, Ong C-N, Ong W-Y, Yu LE. Characterization, purification, and stability of gold nanoparticles. Biomaterials. 2010;31(34):9023-30. http://dx.doi.org/10.1016/j.biomaterials.2010.08.012. PMid:20801502.
39. Massart DL, Vandeginste BG, Buydens LMC, Lewi PJ, Smeyers-Verbeke J, Jong SD. *Handbook of chemometrics and qualimetrics: part A*. Burlington: Elsevier; 1997.
40. Castro KLS, Curti RV, Araujo JR, Landi SM, Ferreira EHM, Neves RS, et al. Calcium incorporation in graphene oxide particles: a morphological, chemical, electrical, and thermal study. Thin Solid Films. 2016;610:10-8. http://dx.doi.org/10.1016/j.tsf.2016.04.042.
41. Ribeiro-Soares J, Cançado LG, Falcão NPS, Martins Ferreira EH, Achete CA, Jorio A. The use of Raman spectroscopy to characterize the carbon materials found in Amazonian anthrosoils. J Raman Spectrosc. 2013;44(2):283-9. http://dx.doi.org/10.1002/jrs.4191.
42. Stobinski L, Lesiak B, Malolepszy A, Mazurkiewicz M, Mierzwa B, Zemek J, et al. Graphene oxide and reduced graphene oxide studied by the XRD, TEM and electron spectroscopy methods. J Electron Spectrosc Relat Phenom. 2014;195:145-54. http://dx.doi.org/10.1016/j.elspec.2014.07.003.
43. Konios D, Stylianakis MM, Stratakis E, Kymakis E. Dispersion behaviour of graphene oxide and reduced graphene oxide. J Colloid Interface Sci. 2014;430:108-12. http://dx.doi.org/10.1016/j.jcis.2014.05.033. PMid:24998061.
44. Kimling J, Maier M, Okenve B, Kotaidis V, Ballot H, Plech A. Turkevich method for gold nanoparticle synthesis revisited. J Phys Chem B. 2006;110(32):15700-7. http://dx.doi.org/10.1021/jp061667w. PMid:16898714.
45. Yongprapat S, Therdthianwong A, Therdthianwong S. Au/C catalysts promoted with metal oxides for ethylene glycol electro-oxidation in alkaline solution. J Electroanal Chem. 2013;697:46-52. http://dx.doi.org/10.1016/j.jelechem.2013.03.003.
46. Kahyaoglu A, Beden B, Lamy C. Oxydation electrocatalitique du glycerol sur electrodes d'or et de platine en milieu aqueux. Electrochim Acta. 1984;29(10):1489-92. http://dx.doi.org/10.1016/0013-4686(84)87033-4.
47. Ribani M, Bottoli CBG, Collins CH, Jardim ICSF, Melo LFC. Validação em métodos cromatográficos e eletroforéticos. Quim Nova. 2004;27(5):771-80. http://dx.doi.org/10.1590/S0100-40422004000500017.
48. Chen W-C, Li P-Y, Chou C-H, Chang J-L, Zen J-M. A nonenzymatic approachfor selective and sensitive determination of glycerol in biodiesel based on a PtRu-modified screen-printed edge band ultramicroelectrode. Electrochim Acta. 2015;153:295-9. http://dx.doi.org/10.1016/j.electacta.2014.12.011.

49. Tremiliosi-Filho G, Gonzalez ER, Motheo AJ, Belgsir EM, Léger JM, Lamy C. Electro-oxidation of ethanol on gold: analysis of the reaction products and mechanism. J Electroanal Chem (Lausanne Switz). 1998;444(1):31-9. http://dx.doi.org/10.1016/S0022-0728(97)00536-6.
50. Borkowska Z, Tymosiak-Zielinska A, Shul G. Electrooxidation of methanol on polycrystalline and single crystal gold electrodes. Electrochim Acta. 2004;49(8):1209-20. http://dx.doi.org/10.1016/j.electacta.2003.09.046.
51. Kadirgan F, Bouhier-Charbonnier E, Lamy C, Léger JM, Beden B. Mechanistic study of the electrooxidation of ethylene glycol on gold and adatom-modified gold electrodes in alkaline medium. J Electroanal Chem Interfacial Electrochem. 1990;286(1-2):41-61. http://dx.doi.org/10.1016/0022-0728(90)85063-B.